NEAR-WALL TURBULENCE STRUCTURES IN THREE-DIMENSIONAL BOUNDARY LAYERS

Anh-Tuan Le, Gary N. Coleman, and John Kim
Department of Mechanical & Aerospace Engineering, UCLA
Los Angeles, California, 90095-1597, USA

ABSTRACT

In this study we examine the structure of near-wall turbulence in three-dimensional boundary layers (3DBLs), which we approximate by applying an impulsive spanwise motion to the lower wall of a turbulent channel flow. Direct numerical simulation (DNS) data are analyzed using Reynolds stress budgets, probability density functions (PDFs) and conditional-averaged quadrant analysis about strong sweeps and ejections, and visualization of vortices with the λ_2 criterion. The evidence suggests that mean three-dimensionality breaks up the symmetry and alignment of near-wall structures, disrupting their 'self-sustaining mechanisms', and thereby causing a reduction in the turbulence kinetic energy (TKE).

INTRODUCTION

In a 3DBL the mean flow direction changes with distance from the wall, and the turbulent stresses are not aligned with the mean shear. In many cases, the result is a decrease in TKE and Reynolds shear stress compared to an equivalent 2DBL. Although 3DBLs exist in which these statistics increase (see listing in Johnston and Flack, 1996), the flowfields in those cases also contain adverse pressure gradients (not a three-dimensional effect), which are known to increase the TKE in the outer regions of the boundary layer. In practice (for example, for the flow over a swept wing) the adverse pressure gradient can dominate over the three-dimensional effects (Coleman, Kim & Spalart, 1997). Even in such flows, however, three-dimensionality serves to damp the turbulence in the near-wall region. And in all cases, the ratio of the turbulent shear stress to the TKE is found to decrease relative to 2DBLs, signifying a reduction in the effectiveness of the turbulence in extracting kinetic energy from the the mean flow.

The mechanism by which the turbulence quantities discussed above are altered has been a subject of much debate. For example, Anderson & Eaton (1989) suggested that the spanwise flow reduces the strength of quasi-streamwise vortices having the opposite sign of streamwise vorticity to the mean spanwise flow, reducing the strong mixing that occurs between vortices of opposite signs. Shizawa & Eaton (1991) found that artificially-generated vortices of either sign embedded into the boundary layer decay faster than they would in a 2DBL, but vortices whose near-wall spanwise velocity is in the same direction as the crossflow produce weakened ejections. Littel & Eaton (1991) found that the crossflow inhibits strong *sweeps* from vortices having near-wall spanwise velocity in the same direction as the crossflow, while it inhibits strong *ejections* from vortices having spanwise velocity in the opposite direction. Kang *et al.* (1998) concluded that the asymmetries in the conditional averages of Littel & Eaton (1991) are only caused by non-Reynolds stress-producing events. Sendstad & Moin (1992) advanced four mechanisms by which the spanwise crossflow affects particle trajectories in the vortical structures, each important at different times, which serve to generate lower Reynolds stress and break up the near-wall streaks. Their findings are, in general, consistent with those of Littel & Eaton. However, the mechanisms described by Sendstad & Moin seem to imply that near-wall vortices are aligned horizontally in the 2D flow, act as independent units on the surrounding fluid, and respond in a two-dimensional manner to the spanwise shear. More recent studies of coherent structures in 2DBLs, both experimental and numerical, indicate that near-wall turbulence structures generally have a finite inclination to the wall, and interact in a cooperative manner to perpetuate turbulence (e.g. Jeong *et al.*, 1997, and Tomkins *et al.*, 1998).

The objective of the present study is to obtain additional insight into the behavior of the near-wall vortical structures which are responsible for the observed changes in turbulence statistics of 3DBLs, by employing some of the new techniques available to analyze the turbulence. The results are expected to be useful in the development of improved turbulence models, and may lead to new techniques for turbulence control.

APPROACH

All solutions described in this paper are obtained using DNS. Various statistical tools, including the Reynolds stress budgets and PDFs, are used to analyze the data. We also employ the conditional-averaged quadrant analysis introduced by Kang, Choi & Yoo (1998). Vortical structures within the flowfields are visualized using the λ_2 criterion of Jeong & Hussain (1995), whereby vortices are associated with negative values of λ_2, defined as the second largest eigenvalue of the tensor $S_{ik}S_{kj}+\Omega_{ik}\Omega_{kj}$, where $S_{ij} = (u_{i,j}+u_{j,i})/2$ and $\Omega_{ij} = (u_{i,j} - u_{j,i})/2$ are the strain and rotation tensors, respectively. Here the subscripts (i,j,k) may have values $(1,2,3)$ which correspond respectively to the streamwise, wall-normal, and spanwise directions, such that $(x_1,x_2,x_3) = (x,y,z)$ and $(u_1,u_2,u_3) = (u,v,w)$.

Our discussion will focus on results obtained by

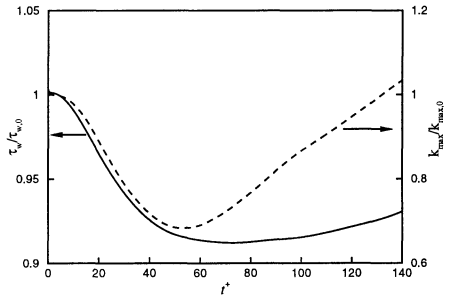

FIGURE 1. History of streamwise wall shear and maximum TKE, normalized by value at initial condition, in channel with spanwise moving wall: ——— τ_w; - - - - k_{max}.

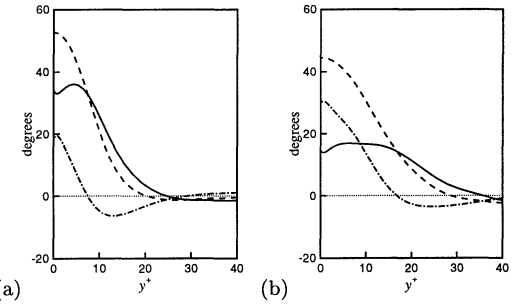

FIGURE 2. Shear angles in channel with spanwise moving wall: - - - - γ_s, mean shear angle; -·-·- γ_τ, turbulent shear angle; ——— λ, lag angle. (a) $t^+ = 13.5$, (b) $t^+ = 27.0$.

the non-stationary 3DBL generated from an impulsive spanwise-moving wall in a fully developed turbulent channel flow. In the interest of demonstrating the generality of the underlying physics, however, we will also discuss statistical results from numerical experiments on the Ekman layer, a statistically stationary 3DBL.

RESULTS

The initial field for this study, at $Re_\tau = 180$, is similar to that of Kim, Moin & Moser (1987), except that a wider domain and greater grid resolution is used to accommodate the resulting realignment of the mean flow caused by the moving wall. At time $t^+ = 0.0$, the wall is set in motion in the spanwise direction with velocity $W_s^+ = -8.5$, generating a spanwise mean shear with positive streamwise vorticity that diffuses outward into the flowfield (we use a '+' superscript throughout to indicate scaling with respect to wall units in the *initial* unperturbed flow).

Turbulence quantities (Reynolds stress, TKE, and stress/energy ratio) initially decrease, then recover (see Coleman, Kim & Le, 1995). A corresponding reduction in streamwise wall shear is observed with a similar time scale (see Figure 1). For the sake of discussion, we will refer to the time interval when the TKE and streamwise wall shear are decreasing ($t^+ < 60$) as the *reduction* period, with *early reduction* being when the rate of decrease is accelerating ($t^+ < 20$), and *late reduction* when the decrease is slowing down ($20 < t^+ < 60$). The period during which the drag and peak TKE increase with time from their minima ($t^+ > 60$) will be referred to as the *recovery* period.

Because we are mainly interested in the mechanisms that reduce turbulence intensity and drag, the present analysis will focus on the changes in the flowfield during the reduction period. Throughout this period, the Reynolds stress and mean shear are not aligned. This misalignment is illustrated in Figure 2 by the lag angle $\lambda = \gamma_s - \gamma_\tau$, where γ_s and γ_τ represent the angles of the mean velocity gradient and turbulent shear stresses, respectively, in the x-z plane reference frame:

$$\gamma_s \equiv \arctan\left(\frac{\partial W/\partial y}{\partial U/\partial y}\right), \quad \gamma_\tau \equiv \arctan\left(\frac{\overline{v'w'}}{\overline{u'v'}}\right).$$

The lag angle can be used to quantify the 'efficiency' of TKE production $P_k = -\left(\overline{u'v'}\partial U/\partial y + \overline{v'w'}\partial W/\partial y\right)$. Using the definitions of γ_s and γ_τ, one can show that $P_k = -\overline{u'v'}^* \frac{\partial U^*}{\partial y}\cos\lambda$, where $\overline{u'v'}^*$ and $\partial U^*/\partial y$ represent the magnitude of the shear stress and mean velocity gradient vectors, $(\overline{u'v'}, \overline{v'w'})$ and $(\partial U/\partial y, \partial W/\partial y)$, respectively. It is evident that when the lag angle λ is nonzero, TKE production is not as efficient as it is in an equivalent 2D flow. And if $\overline{v'w'}$ were to react to the wall motion so that γ_s and γ_τ were of opposite signs, then the negative spanwise production would diminish the total P_k, resulting in even lower production than that in the initial 2D flow. We find this to be true during the early reduction period (see Figure 2), even though the spanwise component's contribution to the TKE production is small at this time. The $-\overline{v'w'}$ budget analysis (see below) reveals that this is caused by the velocity pressure-gradient term becoming larger than the $-\overline{v'w'}$ production immediately after the spanwise shear is imposed by the moving wall.

Reynolds Stress Budget Analysis

Following the notation used by Mansour, Kim & Moin (1988), the Reynolds-stress equations for flow in a plane channel are:

$$\frac{\partial \overline{u_i' u_j'}}{\partial t} = P_{ij} + T_{ij} + D_{ij} + \Pi_{ij} - \epsilon_{ij}$$

where

P_{ij}	$= -\left(\overline{u_i' u_2'} U_{j,2} + \overline{u_j' u_2'} U_{i,2}\right)$	production
ϵ_{ij}	$= 2\overline{u_{i,k}' u_{j,k}'}$	dissipation
T_{ij}	$= -(\overline{u_i' u_j' u_2'})_{,2}$	turb. transport
D_{ij}	$= (\overline{u_i' u_j'})_{,22}$	turb. diffusion
Π_{ij}	$= -\left(\overline{u_i' p'_{,j}} + \overline{u_j' p'_{,i}}\right)$	vel. press-grad. corr.

The budget for the TKE reveals that the production term, $P_k = P_{ii}/2$, has the most influence on the changes in the TKE during the reduction period ($t^+ < 60$), when the near-wall TKE is decreasing (Figure 3). Moin *et al.* (1990) studied a similar 3D channel flow in which the spanwise flow was created by an impulsive constant pressure gradient. In their study, the effective wall velocity increases linearly from zero, rather than being a step function as in the present case. Nevertheless, much of the behavior of the two flows is similar. Moin *et al.* (1990) traced the decrease of TKE production to a

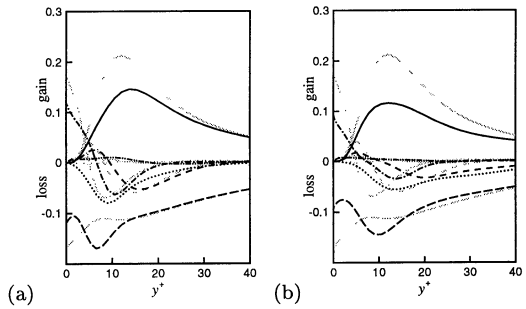

FIGURE 3. TKE budget for channel with spanwise moving wall: ——— production; — — — — dissipation; - - - - turb. transport; -·-·- turb. diffusion; —··— vel. press-grad. corr.; ····· sum of RHS; shaded lines denote initial-condition profiles. (a) $t^+ = 13.5$ (b) $t^+ = 27.0$.

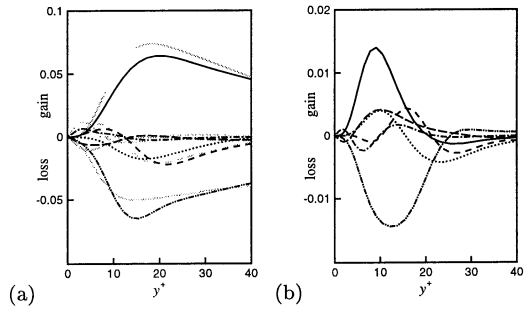

FIGURE 4. Budgets for wall-normal Reynolds stress in channel with spanwise moving wall at $t^+ = 13.5$; symbols same as in Figure 3. (a) $-\overline{u'v'}$ (b) $-\overline{v'w'}$.

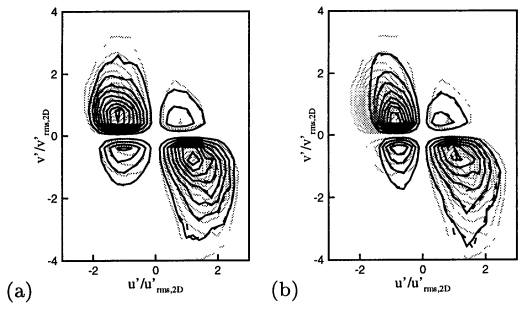

FIGURE 5. Weighted joint PDF of u' and v' in channel with spanwise moving wall at $y^+ = 10$: ——— 3D distribution; - - - - 3D, aligned with γ_τ; shaded lines denote initial-condition contours. (a) $t^+ = 13.5$, (b) $t^+ = 27.0$.

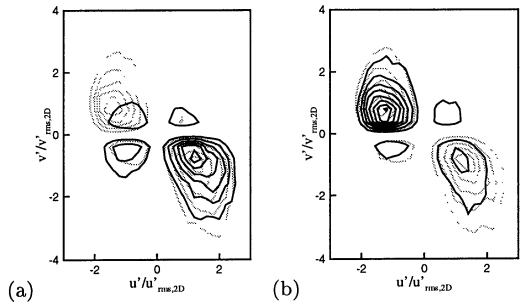

FIGURE 6. Weighted joint PDF of u' and v' in channel with spanwise moving wall at $y^+ = 10$ and $t^+ = 13.5$, conditioned on ω_x: shaded lines denote initial-condition contours. (a) $\omega_x < 0$, (b) $\omega_x > 0$.

reduction in the pressure-strain term in the transport equation for $\overline{v'^2}$, reducing $\overline{v'^2}$ and thus production of $-\overline{u'v'}$ and therefore of TKE. A similar process occurs here: the TKE reduction is accompanied by a drop in Π_{22} (which indicates alteration of the $\overline{v'^2}$ pressure-strain term), which leads to a decrease in $-\overline{u'v'}$ production $-P_{12}$, and ultimately a drop in P_k. For the present flow, however, the crucial chain of events also includes a decrease of $-\Pi_{12}$ for $10 < y^+ < 30$ during the early reduction period (Figure 4a). The velocity pressure-gradient correlation affects $-\overline{u'v'}$ directly, as well as indirectly through $\overline{v'^2}$. The Π_{ij} term is also important in the development of the spanwise stress $-\overline{v'w'}$. The 'new' production $-P_{23}$ introduced by $\partial W/\partial y$ is immediately counteracted by $-\Pi_{23}$. In fact, the magnitude of the latter is larger than that of the former at $t^+ = 13.5$, as shown in Figure 4b. This guarantees that the stress-strain lag angle λ will be nonzero, and thus represents a source of decreased efficiency of the TKE production, as explained above. Turbulence models that accurately depict 3DBLs will need to correctly account (explicitly or otherwise) for the effect of the pressure-velocity correlation terms.

PDF Analysis

Previous 3DBL research demonstrated that turbulent boundary layer structures exhibit asymmetries between the induced flow generated by vortices having the same and opposite signs of vorticity as the spanwise shear layer (henceforth referred to as *positive* and *negative* vortices, respectively). Assertions have also been made that the sweeps and ejections from near-wall vortices are affected in different ways by the three-dimensionality. We seek to verify these findings by examining the PDFs of the velocity field in the 3D channel flow.

Figure 5 shows a weighted joint PDF of u' and v' in the 3D channel at $y^+ = 10$, a location where sweeps and ejections are initially similar in strength, at times $t^+ = 13.5$ and $t^+ = 27.0$. The distribution is weighted by $u'v'$, which reveals how each velocity component contributes to the $-\overline{u'v'}$ shear stress. Because the spanwise fluctuating velocity is slow to respond to the mean spanwise shear, the most important changes to the Reynolds stress early in the flow history are those by the streamwise component $-\overline{u'v'}$. This fact is demonstrated in Figure 5, where the u' and v' distributions in the channel coordinates are essentially the same as those that have been aligned with the Reynolds stress angle γ_τ, implying that the spanwise contribution is insignificant at this time. Figure 5 shows that ejections (events that produce Reynolds stress in the second quadrant, or Q2) are

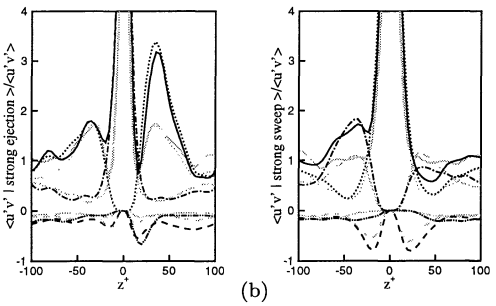

FIGURE 7. Conditional average of $u'v'$ at $y^+ = 10$ in channel with spanwise moving wall, $t^+ = 13.5$: ——— total $\langle u'v' \rangle$; - - - - Q1; —·—·— Q2; ——··— Q3; ····· Q4; shaded lines denote initial-condition contours. (a) strong ejection, (b) strong sweep.

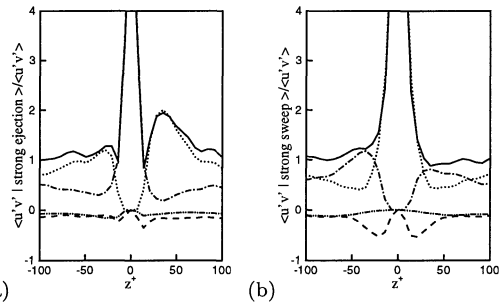

FIGURE 8. Conditional average of $u'v'$ in Ekman layer at $y^+ = 10$; symbols same as in Figure 7. (a) strong ejection, (b) strong sweep.

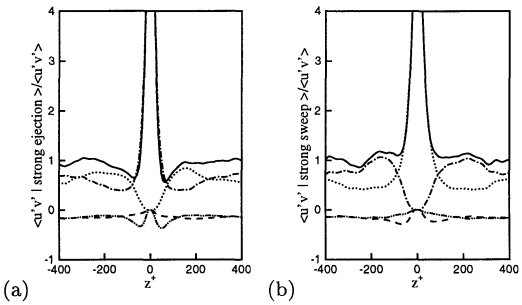

FIGURE 9. Conditional average of $u'v'$ in Ekman layer at $y^+ = 89$; symbols same as in Figure 7. (a) strong ejection, (b) strong sweep.

affected most significantly by reductions in strong negative u', while sweeps (fourth-quadrant, or Q4, events) are affected by reductions in both u' and v'. This result is similar to that of Sendstad and Moin (1992), who attributed the changes in their flow (same as that of Moin *et al.*, 1990) to modification by the crossflow of the trajectories of fluid about streamwise vortices.

To determine the dependence of $-\overline{u'v'}$ on the sign of the streamwise vortex, we condition the weighted joint PDF of u' and v' with the sign of streamwise vorticity. Figure 6 reveals that ejections associated with negative ω_x' are reduced to a much greater extent than the sweeps, while the sweeps associated with positive ω_x' are reduced to a much greater degree than ejections. This is consistent with the findings of Sendstad & Moin (1992) and Littel & Eaton (1991).

Conditional-Averaged Quadrant Analysis

To isolate the important near-wall structures, we examine events that are characteristic of vortical motions. Kang *et al.* (1998) investigated the velocity fields about strong sweeps and ejections in their rotating disk experiment by averaging about locations containing high Reynolds stress, then performing a quadrant analysis on the conditional-averaged quantities. Here, we apply the same procedure to the 3D channel flow.

Figure 7 illustrates the distribution of the Reynolds stress about strong sweeps and ejections at $y^+ = 10$ in the 3D channel, *strong* being defined as events for which $-u'v' > 2u'_{rms}v'_{rms}$, with *sweeps* having $v' < 0$ and *ejections* having $v' > 0$. The center peak in each plot, depicting a strong sweep or ejection, is flanked by two secondary peaks generated by the opposite event. Because near-wall Reynolds stress is for the most part associated with near-wall vortical motion, Kang *et al.* (1998) postulated that the peaks represent the signature of a pair of vortices that generate the strong Reynolds-stress event. In Figure 7a, the left secondary peak represents the sweep of a *negative* vortex ('counter-clockwise' with respect to Figure 7) while the right secondary peak represents the sweep of a *positive* one. Both are dominated by Q4 events. The center peak contains the combined ejections of the negative vortex on the left and positive vortex on the right. Conversely, in Figure 7b the vortices are positive on the left and negative on the right. Note that at $y^+ = 10$ the Q4 events are more pronounced than the Q2 events.

In contrast to the roughly symmetric secondary peaks in the initial 2D field (shown as shaded lines), the 3D flow contains significant asymmetries in both Q2 and Q4 events at $t^+ = 13.5$, resulting in an asymmetric total stress. Specifically, positive vortices generate both stronger sweeps and ejections, or at least are more effective at generating Reynolds stress, than negative vortices. In addition, relative to the plane-averaged $\overline{u'v'}$ at this time, which is decreasing from the 2D level (see Figure 5), strong Q2 and Q4 events are actually stronger, with the strongest events being associated with positive vortices. This suggests that, though there are fewer Reynolds-stress-producing events to contribute to the overall $-\overline{u'v'}$, a greater percentage of the events that do occur generate strong Reynolds-stress. The mean spanwise shear apparently reinforces the effectiveness of positive vortices in generating strong Reynolds shear stress.

The asymmetries observed in the Q2 and Q4 events appear to be in contrast to the findings of Kang *et al.* (1998). However, their measurements were taken at $y^+ \approx 90$, much further away from the wall than in the plots shown here. The 3DBL in their rotating disk experiment is also statistically stationary, rather than time-evolving as in the present study. For more di-

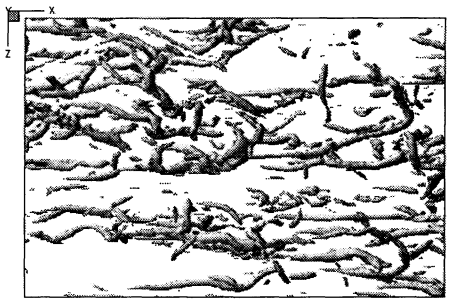

FIGURE 10. Vortices in 2D channel: isosurfaces of $\lambda_2 = -0.012$, scaled with wall units.

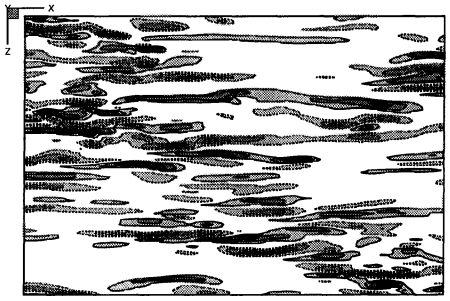

FIGURE 11. Wall-normal vorticity in 2D channel at $y^+ = 5$: ——— $\omega_y' > (\omega_{y,0}')_{rms}$; ····· $\omega_y' < -(\omega_{y,0}')_{rms}$, where $(\omega_{y,0}')_{rms} \equiv (\overline{\omega_y'\omega_y'})^{\frac{1}{2}}$ in initial 2D flow; contour levels incremented by $(\omega_{y,0}')_{rms}$.

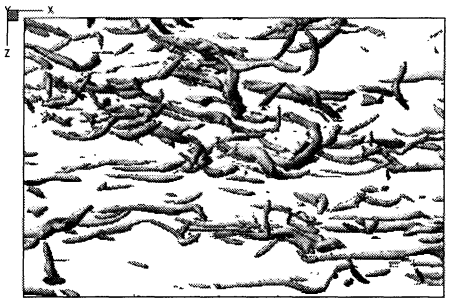

FIGURE 12. Vortices in channel with spanwise moving wall at $t^+ = 13.5$: symbols same as in Figure 10.

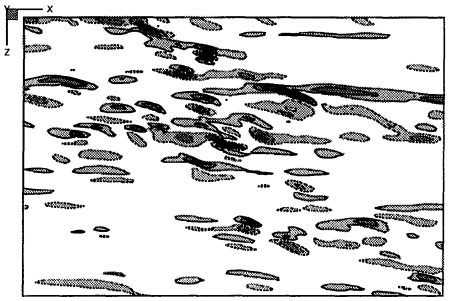

FIGURE 13. Wall-normal vorticity in channel with spanwise-moving wall at $y^+ = 5$ and $t^+ = 13.5$: symbols same as in Figure 11.

rect comparisons, we performed the same conditional average on the Ekman layer of Coleman (1999), also a statistically stationary 3DBL with a similar spanwise mean velocity profile (Reynolds number for this flow is $Re \equiv U_\infty D/\nu = 1000$, where U_∞ is the magnitude of the freestream velocity, and $D^2 = \nu/\Omega$, with Ω being the rate of rotation about the wall-normal axis). Figure 8 reveals that at $y^+ = 10$ the Reynolds stress possesses the asymmetries observed in the channel with a spanwise moving wall, while Figure 9 shows only only a slight asymmetry at $y^+ = 89$, which is more similar to the results of Kang *et al.* (1998). At the larger wall-normal distance, Reynolds stress may not be associated with quasi-streamwise vortices, which exhibit the asymmetric behavior we observe, but with, for instance, the heads of hairpin vortices, which may respond differently to mean three-dimensionality. Certainly, this would explain why the distance between the primary and secondary peaks is much greater in Figure 9 than in Figure 8 (note the expanded horizontal scale in Figure 9).

Visualization

We conclude by visualizing the vortical structures in the channel flow using isosurfaces of λ_2. Figure 10 shows an example for the 2D case. The vortices are oriented roughly in the streamwise direction, and arranged in an overlapping manner. Jeong *et al.* (1997), who performed a conditional average on the λ_2 distribution in a channel flow, described the alignment of the near-wall vortices as the alternating positive-negative pattern illustrated schematically in Figure 14a. Such clustering of vortical structures allows them to reinforce each other's induced flowfields, giving rise to streaks whose lengths are many times longer than the vortices themselves. Figure 11, in which ω_y' contours represent the streak boundaries at $y^+ = 5$, clearly illustrates this fact. Jeong *et al.* (1997) also showed that the 'average' near-wall vortex is not aligned with the x-axis, but is slightly rotated in the x-z plane as shown in Figure 14a, and inclined in the vertical direction, so that the downstream 'head' of the vortex is further away from the wall than the 'tail'.

Figure 12 illustrates the effect of the spanwise shear upon the vortical structures at $t^+ = 13.5$. Although the vortical structures are not diminished to an appreciable degree at this time, the 'tails' of the vortices, which are closer to the wall, move with the wall in the spanwise direction, while the 'heads' remain oriented in the streamwise direction. This results in a change in the shapes of the vortices. Notice that many of the vortices in Figure 12 appear to have more curvature than those in Figure 10, and that the structure of the streaks as shown in Figure 13 appear to be 'breaking up', resulting in a shortened streamwise correlation, and exhibiting some degree of realignment in the new mean flow direction.

Based on the statistical and visualization results, we

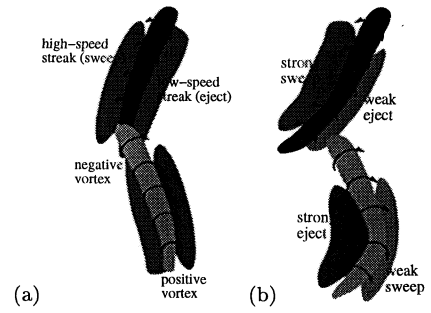

FIGURE 14. Schematic of near-wall turbulence structures in (a) 2DBL and (b) 3DBL.

offer Figure 14b as a model of the changes in vortical structures in a 3DBL. In contrast to the relatively symmetric structures shown in Figure 14a, positive vortices are now 'J-shaped', and negative vortices 'S-shaped'. Because the induced velocity on the concave side of a vortex line is greater than on the convex side, positive vortices create weaker sweeps than ejections, and negative vortices have weaker ejections than sweeps. Moreover, because the single-curvature of a positive vortex would tend to 'focus' its ejections more than the double-curvature of a negative vortex reinforces its sweeps, the Reynolds stress generated by positive vortices would be stronger than that of negative vortices. Another effect of the spanwise shear is to move the vortices away from their cooperative, overlapping alignment, resulting in the break-up of the nearwall streaks, as seen in Figure 13.

In the case of the 3D channel, the TKE, Reynolds shear stress and drag eventually recovers as the near-wall structures realign themselves in the new flow direction. Symmetry is restored in the Reynolds stress production, and the stress-strain lag angle returns to zero. In 3DBLs where mean three-dimensionality is maintained in a stationary state (such as the Ekman layer or the flow over a rotating disk), the lag angle remains finite and the efficiency of the flow in generating turbulence will always be reduced, as implied by the decrease in the stress/energy ratio observed in these flows.

SUMMARY AND CONCLUSIONS

DNS of a channel with a spanwise-moving wall has been used to examine the effects of mean three-dimensionality on near-wall turbulence structures that lead to reduced turbulence intensity and drag. Budget analysis shows that the velocity-pressure gradient correlation acts to oppose production of the Reynolds stresses, resulting in a finite stress-strain lag angle and the diminishing of net TKE production. PDFs and conditional-averaged quadrant analysis results confirm that the three-dimensionality affects positive and negative vortices in different ways, thus destroying the spanwise symmetry of the turbulence structures. Visualizations show that the asymmetries arise due to temporary changes in the shapes of the vortical structures, and the reduction in streak size and strength are due to the alignment of the vortices being altered. These effects reduce the ability of the mean velocity gradient to sustain the turbulence, resulting in the reductions in TKE and drag characteristic of perturbed 3DBLs.

REFERENCES

Anderson, S. C. & Eaton, J. K., 1989 Reynolds stress development in a pressure driven three-dimensional turbulent boundary layer *J. Fluid Mech.* **202**, 263–294.

Bradshaw, P. & Pontikos, N. S., 1985 Measurements in the turbulent boundary layer on an 'infinite' swept wing. *J. Fluid Mech.* **159**, 105–130.

Coleman, G. N. 1999 Similarity statistics from a direct numerical simulation of the neutrally stratified planetary boundary layer. *J. of Atmos. Sci.*, **56**, 891–900.

Coleman, G. N., Kim, J. & Le, A.-T. 1995 A numerical study of three-dimensional wall-bounded flows *Intl. J. of Heat & Fluid Flow*, **17**, 333–342.

Coleman, G. N., Kim, J. & Spalart, P. R., 1997 Direct numerical simulation of decelerated wall-bounded shear flows. *Proc. of 11th Turb. Shear Flows Conf.*, Grenoble, France.

Jeong, J. & Hussain, F., 1995 On the identification of a vortex *J. Fluid Mech.* **285**, 69–94.

Jeong, J., Hussain, F., Schoppa, W. & Kim, J., 1997 Coherent structures near the wall in a turbulent channel flow *J. Fluid Mech.* **332**, 185–214.

Johnston, J. P. & Flack, K. A. 1996 Review – advances in three-dimensional turbulent boundary layers with emphasis on the wall-layer regions. *J. Fluids Engr.* **1.6**, 219–232.

Kang, S. K., Choi, H. & Yoo, J. Y. 1998 On the modification of the near-wall coherent structure in a three-dimensional turbulent boundary layer on a free rotating disk *Phy. of Fluids*, **10**, 2315–2322.

Kim, J., Moin, P. & Moser, R., 1987 Turbulence statistics in fully developed channel flow at low Reynolds number. *J. Fluid Mech.* **177**, 133–166.

Littel, H. S., & Eaton, J. K, 1991 An experimental investigation of the three-dimensional boundary layer on a rotating disk Report No. MD-60, Thermosciences Div., Dept. Mech. Engr., Stanford Univ., Stanford, CA

Mansour, N. N., Kim, J., & Moin, P., 1988 Reynolds-stress and dissipation-rate budgets in a turbulent channel flow. *J. Fluid Mech.* **194**, 15–44.

Moin, P., Shih, T.-H., Driver, D. M. & Mansour, N. N. 1990 Direct numerical simulation of a three-dimensional turbulent boundary layer. *Phys. Fluids* **2**, 1846–1853.

Sendstad, O. & Moin, P., 1992 The near wall mechanics of three-dimensional turbulent boundary layers. Report No. TF-57, Thermosciences Div., Dept. Mech. Engr., Stanford Univ., Stanford, CA

Shizawa, T. & Eaton, J. K, 1990 Interaction of an embedded longitudinal vortex with an attached, three-dimensional turbulent boundary layer. Report No. TF-56, Thermosciences Div., Dept. Mech. Engr., Stanford Univ., Stanford, CA

Tomkins, C. D., Adrian, R. J. & Balachandar, S., 1998 The structure of vortex packets in wall turbulence *Proc. of 29th Fluid Dynamics Conf.*, Albuquerque, NM.